JGR Space Physics

RESEARCH ARTICLE
10.1029/2019JA027006

Can Reconnection be Triggered as a Solar Wind Directional Discontinuity Crosses the Bow Shock? A Case of Asymmetric Reconnection

M. Hamrin[1], H. Gunell[1,2], O. Goncharov[1], A. De Spiegeleer[1], S. Fuselier[3], J. Mukherjee[3], A. Vaivads[4,5], T. Pitkänen[1,6], R. B. Torbert[3,7], and B. Giles[8]

[1]Department of Physics, Umeå University, Umeå, Sweden, [2]Belgian Institute for Space Aeronomy, Brussels, Belgium, [3]Southwest Research Institute, San Antonio, TX, USA, [4]School of Electrical Engineering, KTH Royal Institute of Technology, Stockholm, Sweden, [5]Swedish Institute of Space Physics, Uppsala, Sweden, [6]Institute of Space Sciences, Shandong University, Weihai, China, [7]Space Science Center, University of New Hampshire, Durham, NC, USA, [8]Goddard Space Flight Center, Greenbelt, Maryland, USA

Key Points:
- First observations of externally driven reconnection in the bow shock ramp region
- Asymmetric reconnection could be triggered as a current sheet is compressed at the bow shock
- New type of asymmetry observed: high N and B on one side and supersonic V on other side of X-line

Correspondence to:
M. Hamrin,
hamrin@space.umu.se

Citation:
Hamrin M., Gunell, H., Goncharov, O., De Spiegeleer, A., Fuselier, S., Mukherjee, J., et al. (2019). Can reconnection be triggered as a solar wind directional discontinuity crosses the bow shock? A case of asymmetric reconnection. *Journal of Geophysical Research: Space Physics*, *124*, 8507–8523. https://doi.org/10.1029/2019JA027006

Received 5 JUN 2019
Accepted 23 SEP 2019
Accepted article online 12 OCT 2019
Published online 7 NOV 2019

Abstract Here we present some unique observations of reconnection at a quasi-perpendicular bow shock as an interplanetary directional discontinuity (DD) is crossing it simultaneously with the Magnetospheric Multiscale (MMS) mission. There are no burst data, but available data show indications of ongoing reconnection at the shock southward of MMS: a bifurcated current sheet with signatures of Hall magnetic and electric fields, normal magnetic fields indicating a magnetic connection between the two reconnecting regions, field-aligned currents and electric fields, $\mathbf{E}\cdot\mathbf{J} > 0$ indicating a conversion of magnetic to kinetic energy, and subspin resolution ion energy-time spectrograms indicating ions being accelerated away from the X-line. The DD is also observed by four upstream spacecraft (ACE, WIND, Geotail, and ARTEMIS P1) and one downstream in the magnetosheath (Cluster 4), but none of them resolve signatures of ongoing reconnection. We therefore suggest that reconnection was temporarily triggered as the DD was compressed by the shock. Reconnection at the bow shock is inevitably asymmetric with both the density and magnetic field strength being higher on one side of the X-line (magnetosheath side) than on the other side where the plasma flow also is supersonic (solar wind side). This is different from the asymmetry exhibited at the more commonly studied case of asymmetric reconnection at the magnetopause. Asymmetric reconnection of the bow shock type has never been studied before, and the data discussed here present some first indications of the properties of the reconnection region for this type of reconnection.

1. Introduction

Magnetic reconnection is a fundamental process which allows for a fast conversion of magnetic energy into kinetic energy in current sheets at various regions in space. For example, it is responsible for the explosive release of energy in solar flares (Priest & Forbes, 2002) and geomagnetic storms (Angelopoulos et al., 2008), and it plays a key role for the energy budget of the magnetosphere through reconnection in current sheets at the dayside magnetopause and in the magnetotail (Dungey, 1961). Even though it has been studied extensively (e.g., Paschmann et al., 2013; Wang et al., 2015; Yamada et al., 2014), many unanswered questions remain. For example, what triggers reconnection: can it be triggered when a current sheet is compressed at the bow shock? What are the properties of the diffusion region when the reconnecting regions are far from symmetric and when there is a highly supersonic plasma flow on one side? Here we address these questions by analyzing some unique data from an interplanetary current sheet crossing a quasi-perpendicular bow shock ($\theta > 45°$, where θ is the angle between the bow shock normal and the upstream magnetic field) simultaneously as the Magnetospheric Multiscale (MMS) mission is probing it (Burch et al., 2015).

Current sheets can exist where there are discontinuities, such as tangential and rotational discontinuities, in the magnetic field. However, sometimes it is difficult to determine what type of discontinuity is observed (Neugebauer, 2006), and in the following, they will be denominated directional discontinuities (DDs) without referring to details in the Rankine-Hugoniot conditions. Through simulations, it has been proposed that reconnection could be triggered when an interplanetary DD is compressed by the bow shock (Lin, 1997;

Maynard et al., 2002, 2007). It has even been suggested that the resulting reconnection exhausts could be associated with hot flow anomalies, which are flow anomalies frequently observed near the bow shock (Lin, 1997; Maynard et al., 2002; Paschmann et al., 1988; Schwartz et al., 2000; Thomsen et al., 1986; Zhao et al., 2017).

If reconnection is triggered at the bow shock, signatures of reconnection should be possible to observe at the shock, and even downstream of it if reconnection is continuous. However, thus far, no observational evidence directly from the bow shock has been presented in the literature. Reconnection has been observed at DDs in the pristine solar wind, and it can be recognized as approximately Alfvénic accelerated plasma jets embedded in a bifurcated current sheet (see, e.g.,Gosling, 2012, and references therein). DDs have also been observed to reconnect in the magnetosheath after crossing the bow shock. Maynard et al. (2007) and Phan et al. (2007) reported observations of nonreconnecting solar wind DDs which did reconnect at a later stage when they were observed in the magnetosheath, but it could not be concluded if it was the compression at the bow shock or against the magnetopause which triggered reconnection. Phan et al. (2011), on the other hand, studied a DD which reconnected in the solar wind, but where reconnection had stopped when the DD was observed immediately downstream the bow shock, and then later triggered again as a consequence of the compression against the magnetopause. They argued that reconnection was temporarily disrupted as the DD interacted with the bow shock, but they could not confirm that with direct observations at the shock. Reconnection has also been observed in the downstream turbulent magnetosheath (e.g., Eastwood et al., 2018; Eriksson et al., 2018; Phan et al., 2018; Retinò et al., 2007; Vörös et al., 2017; Wilder et al., 2017, 2018), but without related observations exactly at the bow shock. It is evident that direct observations at the bow shock are needed, together with contextual upstream and downstream data, to investigate what can happen when a DD is compressed by the shock.

In the literature, there are a few reports of reconnection observed near shock ramps (Gingell et al., 2019; Wang et al., 2018). In these cases, reconnection was suggested to arise spontaneously in turbulent magnetic fluctuations in the shock transition region closely downstream the shock ramp, just before the plasma is fully decelerated to the downstream flow. Wang et al. (2018) observed both electron and ion reconnection jets, while Gingell et al. (2019) only observed electron-mode reconnection in the transition region. Such turbulent reconnection has been reproduced in particle-in-cell simulations of perpendicular shocks (Bohdan et al., 2017; Matsumoto et al., 2015) and of the transition and downstream region of a quasi-parallel shock (Bessho et al., 2019; Gingell et al., 2017). The event presented in this article is different from the previous observations by Wang et al. (2018) and Gingell et al. (2019) since it is not driven by nonstationary and spontaneous processes in the turbulent structures at and near the shock, but instead caused by an external driver in the form of a compression of a DD at the shock. Our event is also different from the previous ones since it is observed at the ramp of a quasi-perpendicular bow shock.

Bow shock reconnection is important to study since it corresponds to a case of asymmetric reconnection that has not been studied before. For a long time, much attention has been paid to reconnection where the two reconnecting plasmas are symmetric, for example, in the tail plasma sheet. However, recently, magnetopause reconnection has received more interest, especially since the advent of the MMS missions (Burch & Phan, 2016), and this type of reconnection is asymmetric: the density is significantly higher and the magnetic field strength is significantly lower on the magnetosheath side of the X-line than on the magnetospheric side. Bow shock reconnection, on the other hand, represents another type of asymmetry: now both the density and the magnetic field strength is higher on one side (the magnetosheath) than on the other side (the solar wind). Moreover, on the solar wind side, the plasma flow is also supersonic. For asymmetric reconnection of the magnetopause type, it has been shown that some of the properties of the diffusion region are changed as compared to the case of symmetric reconnection. For example, the stagnation point is displaced away from the high mass flux magnetosheath side and away from the X-line, and the Hall currents and fields are distorted (Eastwood et al., 2013; Pritchett, 2008). The situation becomes even more complicated if there also exists a guide field (Pritchett & Mozer, 2009). What happens to the diffusion region when reconnection is asymmetric of the bow shock type has never been discussed before.

To our knowledge, the data presented in this article are the first in situ observations of possible reconnection when a DD is compressed at the bow shock. The multitude of phenomena at and near the bow shock complicates the data analysis; however, the fact that the DD is observed at a quasi-perpendicular shock, instead of a quasi-parallel one, simplifies the analysis. The article is organized as follows. In section 2, we present

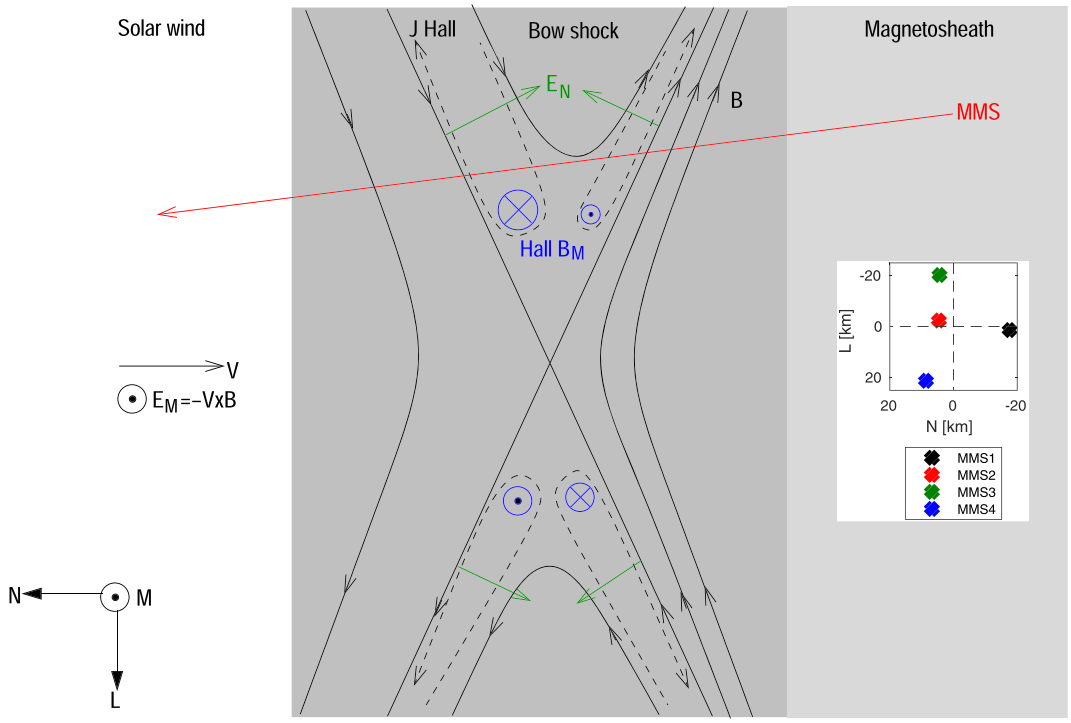

Figure 1. A possible interpretation of the observed data is that Magnetospheric Multiscale (MMS) observes ongoing asymmetric reconnection southward of the effective spacecraft trajectory as the spacecraft cross the bow shock (dark gray region in the figure). The supersonic solar wind comes from the left and the MMS spacecraft cross the suggested reconnection region from the magnetosheath to the solar wind side. The local **LMN** coordinate system of the bow shock is displayed at the bottom left. **L** is approximately southward and **M** duskward. The Hall B_M and E_N fields are shown in blue and green, and the Hall currents by the dashed lines. The inset shows the location of the spacecraft in the **LN** plane. The asymmetry is schematically indicated as denser magnetic field lines on the magnetosheath side of the X line as well as an asymmetric configuration of the Hall fields and currents (only indicated on the northward side of the X line).

the data and instrumentation. The interpretation of the event is schematically summarized in Figure 1, and in section 3.1, we present the MMS observations that are the basis for the interpretation. In section 3.2, we present contextual data from the upstream spacecraft ACE, WIND, ARTEMIS P1, and Geotail as well as the downstream magnetosheath Cluster 4 spacecraft, which all observed the same DD (Angelopoulos et al., 2008; Escoubet et al., 2001). The final section contains a summary and discussion.

2. Data and Instrumentation

The MMS mission with its closely separated spacecraft and outstanding instrumentation offers an unprecedented opportunity to study reconnection at the magnetopause and bow shock (Burch et al., 2015). The MMS mission consists of four spin-stabilized (20-s spin period) spacecraft in an approximately equatorial orbit. We use fast survey mode resolution magnetic field (16 s^{-1}) and electric field (32 s^{-1}) data from the FIELDS investigation, and ion data from the Fast Plasma Investigation (4.5 s/sample; Ergun et al., 2016; Lindqvist et al., 2016; Pollock et al., 2016; Russell et al., 2014; Torbert et al., 2014). MMS was unfortunately not in burst mode during our event, but the survey mode electric and magnetic field data have high enough resolution for a detailed analysis of the DD. The resolution of the Fast Plasma Investigation measurements is, however, too low for resolving the variation of the ion and electron moments in detail over the DD.

We also use ion data from the Hot Plasma Composition Analyzer (HPCA) on board the MMS spacecraft (Young et al., 2016). HPCA takes 0.625 s to make a single energy sweep with 64 energies, stepping from the highest to the lowest energies. However, the energies are decimated by summing over groups of four. HPCA produces a full 3-D ion distribution over half a spin (10 s): 16 energies × 8 elevations × 8 azimuth angles, with energies ranging between 1.74 and 32 keV (center values of summed energies). The energy resolution $\Delta E/E$ is 17%. The energy steps are contiguous (64 total in burst mode). However, for the survey mode data, only

Table 1 Plasma Properties Just Downstream and Upstream the Shock: Magnetic Field, Plasma Density, Speed, Ion Temperature, Inertial Length, Gyroradius, Alfvén Speed, and Plasma Beta

Quantity	Magnetosheath	Solar wind
$\|B\|$ [nT]	51	14
n [cm^{-3}]	80	20
$\|V\|$ [km/s]	150	470
T [eV]	300	50
λ [km]	25	51
ρ [km]	50	73
V_A [km/s]	130	68
β	3.7	2.0

16 energies are brought to ground. These are obtained by summing the counts in four adjacent energy steps. The counts are then distributed evenly over the four energy steps and re-expanded to 64 energies, and over the 16 angle bins. HPCA also delivers high-resolution (subspin) data from single energy sweeps. However, in fast survey mode, the counts from two consecutive sweeps are summed in each energy step, so the actual time resolution of the HPCA subspin data is 1.25 s. Here we specifically use such subspin resolution data from all (omnidirectionally looking) sectors as well as from the sectors pointing approximately north and south (parallel and antiparallel to the spin axis) in the geocentric solar ecliptic (GSE) system. In the fast survey mode, the usual 22.5° angular resolution of HPCA is degraded to 45°. Therefore, also the angular resolution of the observed southward and northward moving ions is 45°. It should be noted that the cold solar wind is not well resolved due to the low angular resolution of HPCA.

Magnetic field data from all four MMS spacecraft are used to estimate the electric current density, **J**, using the curlometer method (Dunlop et al., 2002; Paschmann & Schwartz, 2000). The result is typically more accurate when all tetrahedral faces are close to equilateral, and the relative error in **J** is generally smaller than 10% when the elongation and planarity are $E \lesssim 0.4$ and $P \lesssim 0.4$ (Paschmann & Schwartz, 2000). An often used estimate of the error in the current calculation is the quantity $|\nabla \cdot \mathbf{B}|/|\nabla \times \mathbf{B}|$, where **B** is the magnetic field. In theory, it should be zero, but the value estimated from satellite-based observations can vary substantially from this. An often used upper limit is ~0.5. The scale length of the MMS tetrahedron for this event is ~30 km, which is of the order of, or slightly smaller than, the ion scales (Table 1). The tetrahedron has a small elongation $E \approx 0.14$ and planarity $P \approx 0.29$, implying that the curlometer method should be adequate for determining current densities variations at ~30-km scales (Paschmann & Schwartz, 2000).

In addition to the MMS data, we also use observations of the DD from the upstream solar wind, from the foreshock, and from the magnetosheath. The solar wind data are obtained from the Advanced Composition Explorer (ACE; McComas et al., 1998; Smith et al., 1998), the Wind spacecraft (Lepping et al., 1995; Lin et al., 1995), and the Geotail spacecraft (Frank et al., 1994; Kokubun et al., 1994). From ACE, we use 1-s resolution magnetic field data from the magnetic field investigation (Smith et al., 1998) and 64-s resolution ion moments data from the Solar Wind Electron Proton Alpha Monitor (McComas et al., 1998). From Wind, we use high rate (0.092 s) data from the magnetic field investigation (Lepping et al., 1995) and 3-s resolution on-board ion moments from the 3-D Plasma and Energetic Particle Investigation (Lin et al., 1995). From Geotail, we use 64-s data from the MaGnetic Field experiment (Kokubun et al., 1994) and 96-s resolution plasma moments from the Comprehensive Plasma Instrument/Solar Wind Analyzer (Frank et al., 1994). Data from the foreshock and from the magnetosheath are obtained by the mission ARTEMIS P1 spacecraft (Angelopoulos, 2008) and by the Cluster 4 spacecraft (Escoubet et al., 2001), respectively. From ARTEMIS P1, we use 0.0625-s resolution magnetic field data from the FluxGate Magnetometer (Auster et al., 2008) and on-board plasma moments (~4.3 s) from the ElectroStatic Analyzer (McFadden et al., 2008). From Cluster, we use full resolution (~0.05 s) magnetic field data from the FluxGate Magnetometer (Balogh et al., 2001) and spin resolution (~4 s) proton moments from the Cluster Ion Spectrometry experiment/COmposition Distribution Function (Rème et al., 2001). The ACE, Wind, Geotail, and ARTEMIS data are retrieved from the Coordinated Data Analysis Web, while the Cluster data are retrieved from the Cluster Science Archive.

3. Observations

3.1. MMS Observations at the Bow Shock

On 19–20 December 2015, MMS observed several bow shock crossings. See Figures 2a–2e, where the crossings are observed as transitions between the cold, low density, and high speed solar wind, and the lower speed shocked magnetosheath plasma with increased density and magnetic field strength. All shocks observed 22:55–03:30 UTC are of quasi-perpendicular type, with an angle 80°–125° between the upstream interplanetary magnetic field (IMF) and the mixed mode bow shock normal (Paschmann & Schwartz, 2000).

A zoomed plot of the last two bow shock crossings is presented in Figures 2f–2j. MMS enters from the undisturbed solar wind into the magnetosheath at ~03:26:14 and exits into the solar wind again at ~03:27:48 at $[X_{GSE}, Y_{GSE}, Z_{GSE}] \approx [11.1, -4.1, -1.0]R_E$. A solar wind DD is crossing the shock at the same time as MMS is probing it. The DD is observed at about 3:27:47.4–03:27:49.7 and it is highlighted in yellow in Figures 2f–2j.

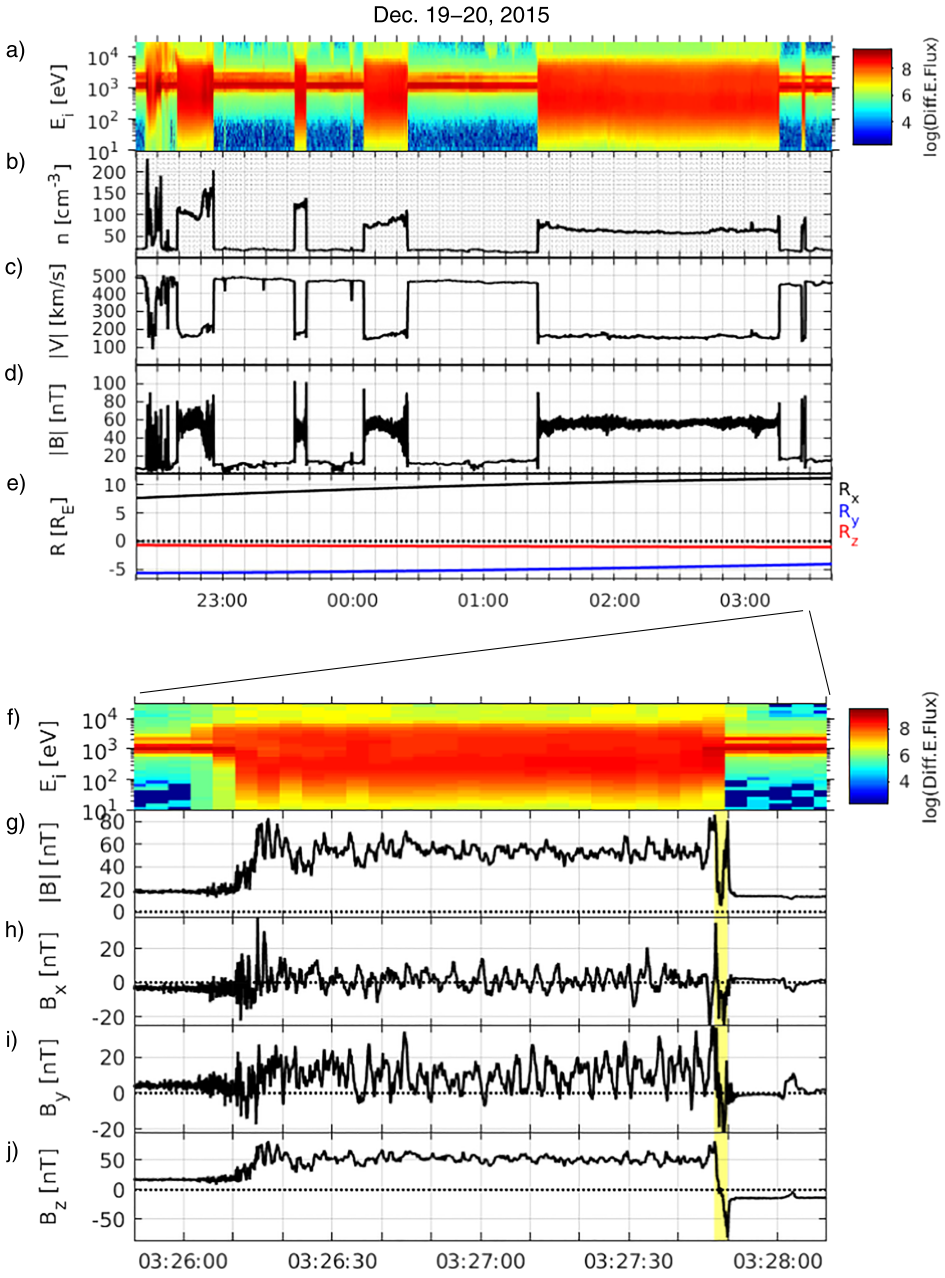

Figure 2. Magnetospheric Multiscale 1 bow shock crossings on 19–20 December 2015. (a) Fast Plasma Investigation ion energy-time spectrogram, (b) ion density, (c) ion speed, (d) magnetic field magnitude, and (e) spacecraft position. (f–j) Zoom onto the last two crossings. Data are presented in the geocentric solar ecliptic system. The event at 03:27:47.4–03:27:49.7 UTC is highlighted in yellow, and it is associated with a directional discontinuity crossing the bow shock.

The discontinuity is evident from the sign change of B_z in Figure 2j. The magnetic field upstream and downstream from the shock are approximately [2.0, −1.4, −14] nT and [0,10, 50] nT, respectively, corresponding to an almost complete rotation (170° rotation) in the magnetic field direction over the DD. The Alfvén Mach number just upstream this bow shock crossing was ~7.

The DD is embedded within the bow shock (approximately 03:27:47–03:27:50.5 UTC). The first encounter of the solar wind with the bow shock is at the beginning of the shock foot at ~03:27:50.5 UTC. Downstream from the foot, $|B|$ exhibits oscillations due to the rapid change in B_z at the DD as well as due to the turbulent nature of the magnetosheath and the typical over-undershoot behavior behind a quasi-perpendicular bow

shock (Bale et al., 2005). The ramp region is evident from the rapid increase in $|B|$ and decrease in B_z. It corresponds to an electric current flowing along the shock surface toward dawn (along $-y_{GSE}$), and it is caused by the reflection of ions and electrons in the enhanced shock magnetic field (Bale et al., 2005). Table 1 contains some approximate properties of the plasma just before and after the shock. Note that the properties upstream and downstream of the DD are significantly different, and any possible reconnection at the DD embedded in the bow shock has to be asymmetric.

The data are analyzed in detail in the local coordinate system of the DD at the shock. However, determining the exact orientation is complicated for several reasons, for example, waves in the shock region and the magnetosheath. Here, we determine the orientation of the DD at the shock ramp using a combination of methods similar to Retinò et al. (2007) who determined the orientation of a reconnecting current sheet embedded in the magnetosheath. We use the normal direction from multi-spacecraft timing of the magnetic field observed by all four spacecraft and the maximum variance direction from MVA on the magnetic field observed by MMS 1 (Schwartz, 1998). We obtain $\mathbf{L} = [-0.19, 0.09, -0.96]$, $\mathbf{M} = [0.06, 0.97, 0.08]$, and $\mathbf{N} = [0.98, -0.04, -0.20]$. The timing speed is ~170 km/s, and we see that **N** and **L** are approximately along X_{GSE} and $-Z_{\mathrm{GSE}}$. The orientation of the four MMS spacecraft in the **LN** plane is indicated in the inset in Figure 1.

Figure 3 shows the magnetic and electric fields and derived quantities. The B_L reversal of the DD is observed by all spacecraft and it is highlighted in yellow. B_L changes in two steps over the DD with an approximately flat region at the center. This suggests that the current sheet of the DD is bifurcated into one part facing the magnetosheath ($\mathrm{CS_{MS}}$) and one facing the undisturbed solar wind ($\mathrm{CS_{SW}}$). The approximate center of each current sheet are indicated with the dashed lines. All spacecraft observe rather similar signatures, but the B_L magnetic field gradient is steeper at the magnetosheath current sheet. This is possibly an effect of asymmetric reconnection. For example, in the case of asymmetric magnetopause-like reconnection, the current sheet is compressed away from the region of higher dynamic pressure (Eastwood et al., 2013; Pritchett, 2008; Pritchett & Mozer, 2009).

B_M is large, of the order of B_L (Figure 3b). It shows a bipolar signature between the two current sheets $\mathrm{CS_{MS}}$ and $\mathrm{CS_{SW}}$. This is typical for the Hall magnetic field in the ion diffusion region of reconnection. On the solar wind side, all spacecraft observe a peak at ~03:27:49.2, while the peak at the magnetosheath side (around 03.27:47.6) is observed at slightly different times by the four spacecraft. Note that the bipolar signature is not evenly distributed over the event. Instead, the peak is wider at the solar wind side and narrower at the magnetosheath side. This is similar to the results from simulations of asymmetric magnetopause-like reconnection where B_M is compressed and confined to a narrower region away from the region of higher dynamic pressure (Pritchett, 2008; Pritchett & Mozer, 2009). Between the bipolar peaks, we see possible signatures of a reconnection guide field ~ -10 nT when averaging over the four spacecraft. A combination of asymmetric reconnection and a nonzero guide field is known to cause additional distortions to the Hall fields (Eastwood et al., 2013).

The normal component B_N is negative between the two B_L peaks (Figure 3c). A nonzero value of B_N at the center of the event indicates a magnetic connection between the oppositely directed magnetic field regions of the DD. All spacecraft agree on $B_N < 0$ but they observe different magnitudes. Moreover, there is a positive B_N peak observed by MMS 1, 3, and 4 on the magnetosheath side of $\mathrm{CS_{MS}}$. These signatures are likely due to ripples in the bow shock or other spatial and temporal variations of the bow shock (e.g., Johlander et al., 2016) which cause disturbances of the DD and variations in the signatures observed by the spacecraft as the DD crosses over them. (For example, the size and position of the positive B_N peak changes depending on where/when the **LMN** system is determined: in the case presented in Figure 3, **LMN** is obtained on the shock ramp and the positive B_N peak is observed before $\mathrm{CS_{MS}}$. On the other hand, obtaining **LMN** at $\mathrm{CS_{MS}}$, the positive B_N is instead observed after $\mathrm{CS_{SW}}$ [data not shown].)

The magnetic field strength is shown in Figure 3d. We see that the pile-up of the magnetic field at the shock ramp ($B_L > 0$) is visible just to the right of the yellow region, and it corresponds to a dawnward current, that is, in the $-\mathbf{M}$ direction. When mentioning this, it is also worth noticing that $\mathrm{CS_{MS}}$ is part of a "remnant" bow shock ramp which existed previously when the IMF was oppositely directed. The DD is hence observed in a region close to the ramp, approximately between the remnant ramp and the newly formed ramp. The magnetic field magnitude is small between $\mathrm{CS_{MS}}$ and $\mathrm{CS_{SW}}$, while inside the magnetosheath (before ~03:27:47.3 UTC), $|B|$ is large and fluctuating. The smallest values of $|B|$ inside the event are observed by MMSs 1 and 3, which indicate that these spacecraft are closest to a magnetic null. MMS 4 observing a larger

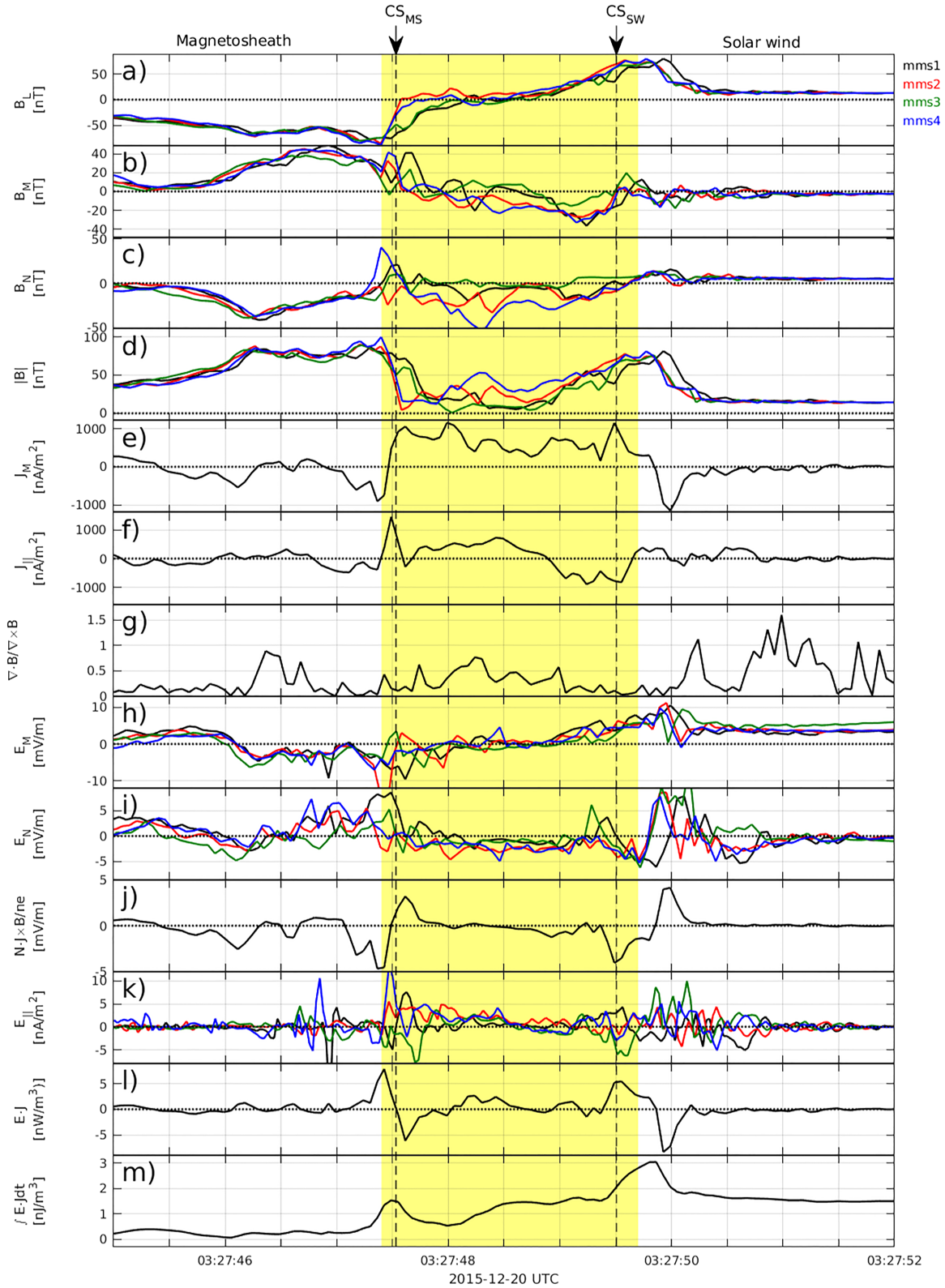

Figure 3. Zoom onto the directional discontinuity (yellow) embedded in the bow shock. The magnetosheath is to the left and the undisturbed solar wind to the right. The approximate center of the two parts of the bifurcated current sheet are indicated with the dashed lines. (a–d) **LMN** components and magnitude of the magnetic field, (e–f) current density along **M** and along the magnetic field, (g) quality estimate of the curlometer, (h–i) **M** and **N** components of the electric field, (j) normal component of the Hall term of the generalized Ohm's law, (k) the parallel electric field, and (l–m) the power density and its integral along the spacecraft path.

value of $|B|$ at the time it probes the center of the event is possibly due to temporal and spatial variations on the shock as discussed above. The region of the smallest magnetic field magnitudes is observed closer to the magnetosheath side of the bifurcated current sheet. A similar displacement of the magnetic null away from the region of larger dynamic pressure has been observed in simulations of asymmetric magnetopause-like reconnection (Pritchett, 2008; Pritchett & Mozer, 2009).

The variation of the magnetic field over the event with a B_L reversal (negative to positive along the spacecraft path), a large and bipolar B_M (positive to negative), a negative B_N, and a small $|B|$ at the center suggests that MMS probed the ion diffusion region northward of an X-line embedded in the bow shock near the ramp. In Figure 1, we present a schematic sketch of reconnection adapted to the configuration of the event. In this case, reconnection has to be asymmetric since the two reconnecting plasmas are distinctly different (and even with a supersonic flow on one side), but the asymmetry is only schematically indicated in the figure. The inset shows the location of the spacecraft in the **LN** plane.

Assuming that the entire structure (03:27:47.4–03:27:49.7 UTC) propagates approximately at the timing speed of ~170 km/s, its thickness would be about 390 km or $10\lambda_i$, where an average ion inertial length of ~39 km has been used (Table 1). We obtain an estimate of the angle between the separatrices according to $|B_L/B_N| \approx 70/10$ (Figures 3a and 3c), which implies that the spacecraft should cross the diffusion region $\sim 70\lambda_i$ away from the X-line (Priest & Forbes, 2002). However, Hall fields have been shown to persist far away from the X-line . For instance, there are examples of Hall fields being $\sim 1,000\lambda_i$ away from the X line in the solar wind (Mistry et al., 2016) and $\sim 100\lambda_i$ away from the X line in the magnetosheath (Eastwood et al., 2018). Moreover, $B_N \approx 0.14B_L$ implies a fast reconnection rate (Priest & Forbes, 2002).

Results from the curlometer method are presented in Figures 3e–3g. We see that $|\nabla \cdot \mathbf{B}|/|\nabla \times \mathbf{B}|$ is mostly smaller than 0.5 over the event (Figure 3g), indicating that the error in the current density should be limited (Paschmann & Schwartz, 2000). The out-of-plane current J_M is large and positive inside the event (Figure 3e). The signature of a bifurcated current sheet is evident from the minimum in J_M in the middle of the event. The negative excursion of J_M at the shock ramp corresponds to the dawnward current (along -**M**) needed to create a $\mathbf{J} \times \mathbf{B}$ force that decelerates the incoming solar wind plasma, and the oscillations in J_M inside the magnetosheath are possibly due to the overshoot and undershoot magnetic field signatures and trapped ions behind the shock (e.g., Bagdonat & Motschmann, 2002; Bale et al., 2005; Lindkvist et al., 2018; Saxena et al., 2005; Vernisse et al., 2018).

The field-aligned current density component, $J_{\parallel}$, is presented in Figure 3f. At CS_{MS}, there is a strong and narrow peak with $J_{\parallel} > 0$ followed by a short interval with $J_{\parallel}$ weakly negative. Thereafter, $J_{\parallel}$ is positive but it turns negative at ~ 03:27:48.9, and it stays negative all the way through CS_{SW}. $J_{\parallel}$ hence has an orientation similar to what is expected for the Hall currents of reconnection (Figure 1), but it is substantially distorted from the classical picture of symmetric reconnection. In the case of magnetopause-like asymmetric reconnection, $J_{\parallel}$ has shown to be distorted (Pritchett & Mozer, 2009).

The out-of-plane electric field, E_M, in the frame of the DD is presented in Figure 3h. On the solar wind side of the DD, $E_M \approx 3$mV/m (in the frame of the DD), corresponding to an $\mathbf{E} \times \mathbf{B}/B^2$ convection toward the reconnection region. On the other side, E_M is close to zero or even negative, implying negligible inflow (but further downstream before ~03:27:46 $E_M \approx 3$mV/m again). The flow into a reconnection site is known to either be spontaneous or driven by external processes (Gosling, 2012). In our case, it is likely that the apparent one-sided inflow is caused by the impinging and highly supersonic solar wind. It should also be noted that the value of E_M is sensitive to the exact value of the velocity used for the transformation to the DD frame, and a separate analysis (not shown) indicates that variations in the velocity can alter the value of E_M at the magnetosheath, but without changing its sign. Inside the main part of the event (03:27:48–03:27:49.9 UTC), E_M is on the average positive. Together with $J_M > 0$, we thus have $\mathbf{E} \cdot \mathbf{J} > 0$, which is needed for converting magnetic energy to kinetic energy through reconnection.

The normal electric field E_N in Figure 3i is varying, but it is on the average positive (negative) at CS_{MS} (CS_{SW}). Such a variation is consistent with a Hall electric field (Figure 1). We see that $|E_N| \approx 5$ mV/m in the DD frame and extending over ~0.3 s (or ~50 km using the DD speed of ~170 km/s). Ions accelerated over such a potential drop would hence gain an energy of ~260 eV. Figure 3j shows the normal component of the Hall term of the generalized Ohm's law, $\mathbf{N} \cdot (\mathbf{J} \times \mathbf{B})/(en)$, where n is the plasma density and e the elementary charge. There is an approximate consistency between the directly measured E_N and $\mathbf{N} \cdot (\mathbf{J} \times \mathbf{B})/(en)$, even

though the magnitude of E_N is slightly larger. This indicates that a substantial part of E_N at the bifurcated current sheet is balanced by the Hall term. However, fluctuations in the turbulent magnetosheath and near the bow shock may cause additional electric field disturbances. Moreover, the lower resolution of the density estimate n as compared with **J** and **B** may reduce the magnitude of the estimated Hall term. Note also that there is a positive excursion of the electric field at the shock ramp just before the DD (Figures 3i–3j). This corresponds to the electric field decelerating the incoming solar wind. The electric field in the ramp region is also rather well balanced with the Hall term, which is consistent with previous observations (Eastwood et al., 2007).

In Figure 3k, we show the observed $E_{\parallel}$ in the frame of the shock. $E_{\parallel}$ is highly varying and there are strong parallel fields at the ramp and at CS_{MS} and CS_{SW}. According to simulations of magnetopause-like asymmetric reconnection, the structure of $E_{\parallel}$ is quite diffuse and patchy, but there should exist parallel electric fields generally pointing away from the X-line (Pritchett, 2008). This is consistent with Figure 3k, where we see a tendency of $E_{\parallel} > 0$ at CS_{MS} and $E_{\parallel} < 0$ at CS_{SW} (cf. Figure 1 and note the opposite direction of the magnetic field at the two sides of the X line).

The energy conversion between the fields and the particles can be analyzed through the term $\mathbf{E}\cdot\mathbf{J}$ (Figure 3l). We see that $\mathbf{E}\cdot\mathbf{J} > 0$ over the main part of the event (03:27:48–03:27:49.7 UTC), corresponding to an energization of the plasma. On the other hand, at the shock ramp, $\mathbf{E}\cdot\mathbf{J} < 0$, which is consistent with the deceleration of the incoming solar wind. At the magnetosheath edge of the DD, $\mathbf{E}\cdot\mathbf{J}$ is varying, possibly due to a combined effect of plasma acceleration in the diffusion region and a plasma deceleration at the remnant bow shock ramp near CS_{MS}. To further investigate the energy transfer over the event, we compute the integral along the spacecraft path, approximated as a cumulative sum multiplied by the sampling time (Figure 3m). We see that the integral over the main part of the event (03:27:48–03:27:49.7 UTC) is about +2.5 nJ/m^3, while near CS_{MS} (03:27:47.4–03:27:47.6) it is ∼0, and over the bow shock ramp (03:27:49.8–03:27:50) about −1 nJ/m^3. Inspecting the entire bow shock crossing including also the ramp (about 03:27:47.4–03:27:50), the integral is ∼1.5 nJ/m^3, that is, corresponding to an overall energization of the plasma. This can be compared to the other bow shock crossings (Figure 2a–2e) where the integral is found to be in the range −20 to −2 nJ/m^3 (not shown), that is, instead a transfer of energy from the particles to the fields which is typical for a bow shock.

The energization of the plasma is also investigated with subspin-resolution HPCA data, and the HPCA data can strengthen our conclusions about ongoing reconnection southward of the MMS spacecraft as obtained from signatures in the electric and magnetic field data and derived quantities (Figures 1 and 3). In Figure 4, we present data from MMSs 1, 2, and 3 (no HPCA data are available from MMS 4) of the HPCA energy-time spectrogram for ions moving approximately northward, southward, and omnidirectionally using the available HPCA sectors (see section 2) as well as the **LMN** components of the magnetic field. In Figures 4a, 4e, and 4i, we indicate with crosses a simple approximation of the mean energy of the observed northward moving ion distribution (computed as a weighted average, weighted by the ion flux) in the magnetosheath proper and in the region of the DD. In the omnidirectional data (Figures 4c, 4g, and 4k), we can see traces of the incoming solar wind (remember that HPCA does not resolve the cold solar wind well due to the limited angular resolution). It can be observed as a narrow and faint population at ∼1 keV corresponding to ∼450 km/s. The incoming solar wind is best resolved by MMS 2 (Figure 4g). Inside the magnetosheath proper, before ∼03:27:45 UTC, in the energy-time spectrograms, we see a broad distribution with high ion fluxes extending over a large energy interval reaching from small energies below 10 eV and falling off under $\sim 10^5$ (cm^2 s sr eV)$^{-1}$ at a few hundred eV (Figures 4a, 4e, and 4i). This is typical for the magnetosheath. This is the distribution that previously has been decelerated and heated at the upstream bow shock before the DD arrival.

When comparing the distribution inside the DD with the distribution in the magnetosheath proper, for MMS 1, we see that the northward ion distribution is elevated in energy in the two bins 03:27:46.6–03:27:49.1 UTC (marked with arrows in Figure 4a). Now the high flux falls off under $\sim 10^5$ (cm^2 s sr eV)$^{-1}$ at several hundreds of eV, corresponding to a 200–300 eV lift of the distribution as compared with the magnetosheath proper discussed in the previous paragraph. Also the flux at low energies (<10 eV) is much smaller than in the magnetosheath proper in these two bins. In addition to the expected deceleration and heating of the plasma at a typical bow shock, the lifted ion distribution in our case should correspond to an additional energization process at the shock. The energization of the ions can also be observed from the estimates of the average upward energy (crosses in Figure 4a), and we find that the average energy is

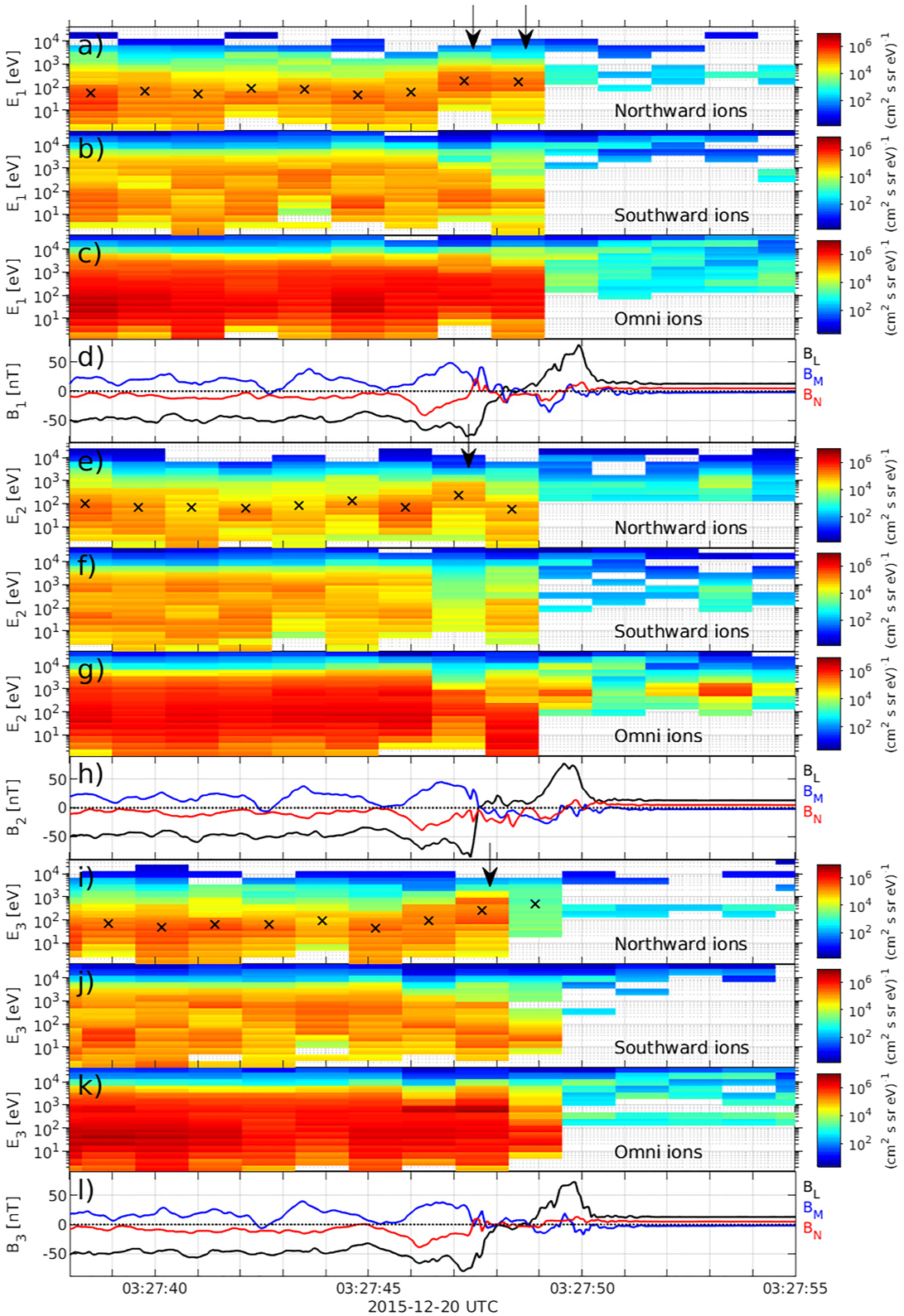

Figure 4. Hot Plasma Composition Analyzer energy-time spectrogram for (a) northward moving, (b) southward moving, and (c) approximately omnidirectional ions (using all available sectors) as well as (d) **LMN** components of the magnetic field observed by Magnetospheric Multiscale (MMS) 1. (e–l) Same data format but from MMSs 2 and 3, respectively. The crosses indicate the average energy of northward moving ions in the magnetosheath proper and in the region of directional discontinuity (see the text for details). The bins where the northward ion population is lifted in energy are indicated with arrows. See the text for a discussion.

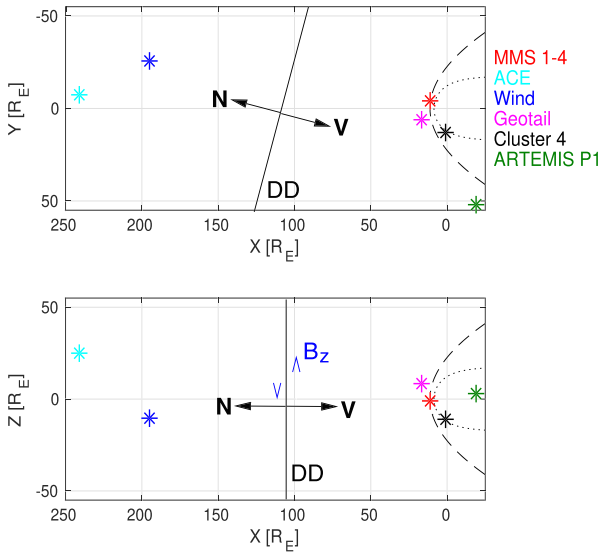

Figure 5. Missions observing the directional discontinuity (DD). The dashed and dotted lines show the approximate location of the bow shock and magnetopause in the geocentric solar ecliptic system (Farris & Russell, 1994; Shue et al., 1997). The DD is schematically indicated in the upstream solar wind together with its approximate normal direction and the reversal in B_z.

increased by one or a few hundred eV in the two bins at the DD, that is, slightly smaller than the observed 200–300 eV lift of the high energy part of the distribution as discussed above. However, note that it is difficult to determine an accurate value of the average energy due to the limited HPCA energy resolution and due to the fact that the estimate is based only on data from a few HPCA sectors (see section 2). Moreover, it should also be noted that from our HPCA data with limited resolution, it is not possible to obtain any accurate estimates of the moments of the ion distribution, that is, the bulk flow and temperature. We can hence not draw any conclusions about how much of the additional ion energization at the DD that corresponds to a bulk acceleration of the ions and a temperature increase, respectively.

A similar lift in the northward ion distribution is also observed by MMSs 2 and 3 in the next-to-last bin before the approximately undisturbed solar wind. These bins are marked with arrows in Figures 4e and 4i (note that the flux in the ~03:27:49 UT bin for MMS 3 in Figure 4i is so low that it is difficult to draw any conclusions about that bin). Moreover, the southward distribution for MMSs 1, 2, and 3 shows no signs of such an energy lift at the DD (Figures 4b, 4f, and 4j). Instead, it falls off at the DD so that the distribution here becomes confined to a smaller low-energy range. This is similar to the distributions (both northward and southward) observed at all the other bow shock crossings in Figure 2 (data not shown). For MMS 2, there is even a drop-out in the southward distribution at the arrow. The energy lift in the northward distributions obtained by MMSs 1, 2, and 3 is unlikely to be caused by ions reflected and accelerated at the quasi-perpendicular bow shock (Bale et al., 2005). Such reflected ions should be observed in the foot region of the shock, that is, upstream the observed DD, and they should propagate in a direction perpendicular to the shock normal and the IMF, that is, approximately toward dusk in our case. Indeed, in the omnidirectional data near and after ~03:27:50 (Figures 4c, 4g, and 4k at $\gtrsim$10 keV), we see indications of such a reflected and accelerated ion population. We therefore suggest that our HPCA observations at the arrows are consistent with an ion energization and a reconnection exhaust from an X-line southward of the spacecraft (Figure 1), but how much of the energization that corresponds to heating is not possible to determine from our data. However, it has been shown that ions crossing the separatrix region into the exhaust gain both a directed flow and a thermal speed (e.g., Drake et al., 2009). We hence argue that our observations are consistent with an ion acceleration and energization over the potential drop of ~260 eV at CS_{MS} and CS_{SW} as estimated from E_N (Figure 3i–3j, see the discussion above).

3.2. Upstream and Downstream Observations

The DD is observed by five other missions (Figure 5): ACE and Wind in the upstream undisturbed solar wind, Geotail close to the subsolar nose point of the bow shock, ARTEMIS P1 in the quasi-parallel foreshock

region at the dusk flank (the angle between the IMF and the Farris bow shock normal at ARTEMIS P1 is about 20° Farris & Russell, 1994), and Cluster 4 in the dusk magnetosheath. Magnetic field, plasma velocity, and density data from the spacecraft are presented in Figure 6 and some key observables are listed in Table 2.

The DD is clearly visible from the B_z reversal observed by all spacecraft (top panels in Figures 6a–6e). However, the sampling frequency differs between the spacecraft, and Geotail barely resolves the DD in the magnetic field. The magnetic shear angle is 110° –170° , with the largest angles observed by the ACE and Wind missions in the upstream undisturbed solar wind (Table 2). Note that the spacecraft observe a slightly different shape of the DD, with a bump in B_z observed near the center of the DD, especially for ACE and Cluster. This indicates that the shape of the DD varies or evolves over the large spatial and temporal scales spanned by the five spacecraft. The positive excursion of B_z observed by Geotail and ARTEMIS about 2 min after the DD is likely associated to the magnetic field flip observed at ∼02:34:00 UTC by ACE and ∼02:44:43 UTC by Wind. The resolution of the plasma moments are low for all missions, so the detailed variation of the velocity and density over the DD cannot be resolved in detail.

It can also be noted that the B_y component is observed to be somewhat different at the various spacecraft. Wind and MMS observe a change in B_y from positive to negative across the DD, while ACE, Geotail, ARTEMIS, and Cluster observe $B_y > 0$ both before and after the DD (Figures 2 and 6). This is consistent with MMS and Wind observing an almost complete rotation of the magnetic field (∼ 170°) at the DD as compared to ACE (∼ 140°), and Geotail, ARTEMIS, and Cluster (∼ 110–130°, see section 3.1 and Table 2). Moreover, all of the spacecraft except ARTEMIS observe signatures of $B_y \leq 0$ inside the DD. Wind is the most dawnward spacecraft (its closest neighbor is the upstream monitor ACE which is located more than $18R_E$ away along Y), and ARTEMIS is the most duskward one (Figure 5). One possibility for the different B_y observations are spatial and temporal variations between the spacecraft. However, the spatial volume probed by the entire spacecraft fleet is very large, as can be seen in Figure 5, and it is only possible to speculate about the reason for the variation of the B_y observations between the spacecraft.

The observed solar wind speed upstream of the bow shock is V_x ∼450 km/s but it varies slightly between the spacecraft (fourth panels in Figures 6a–6d). This variation can be due to fluctuations in the solar wind velocity as well as due to measurement errors in the spacecraft's plasma moments (note the low resolution of the moments). Using multi-spacecraft timing analysis (Paschmann & Schwartz, 2000) on the magnetic field data from ACE, Wind, Geotail, and ARTEMIS, we obtain a propagation speed of ∼430 km/s which is close to the observed wind velocity.

Using MVA on the magnetic field data, we compute the **LMN** directions of the DD at the five spacecraft (Table 2). For Geotail, these directions are very approximate due to the low resolution of the data. The definition of **N** has been chosen consistently with the outward bow shock normal at MMS, implying that the DD propagates antiparallel to **N** (Figure 5). All spacecraft observe a dominant X_{GSE} component of **N**. Upstream ACE and WIND as well as downstream Cluster and ARTEMIS also observe a significant $-Y_{\mathrm{GSE}}$ component. Geotail, on the other hand, observes a $+Y_{\mathrm{GSE}}$ component. This may be due variations in the DD orientation between the spacecraft, but it is not possible to confirm due to the very low resolution of the data. At MMS, the orientation of the DD has changed so that **N** is approximately directed along X_{GSE} (section 3.1), which is consistent with the DD being compressed at the bow shock at its approximate nose point. That the DD becomes compressed at the bow shock is also evident from the size of B_L at the reversal: at ACE, Wind, Geotail, and ARTEMIS, B_L flips ∼ ±13 nT, while at MMS, it flips ∼ ± 70nT, and at Cluster, ∼ ±50 nT.

The duration of the DD is of the order of 2 min as observed by ACE, Wind, and Geotail, while ARTEMIS, Cluster, and MMS observe a thinner DD (∼15, ∼6, and ∼2.3 s). The variation in the DD duration is likely caused by variations in the DD between the spacecraft, and it is possible that the DD evolves and steepens closer to the Earth (MMS and Cluster) and behind it (ARTEMIS). However, the low resolution of the data, especially from Geotail, makes it difficult to accurately estimate the DD duration.

4. Summary and Discussion

In this article, we have presented some unique data of an interplanetary DD crossing a quasi-perpendicular bow shock at the same time as MMS was probing it. The amount of available data is limited since there are no burst data for this event. Nevertheless, the MMS electric and magnetic field data show indications

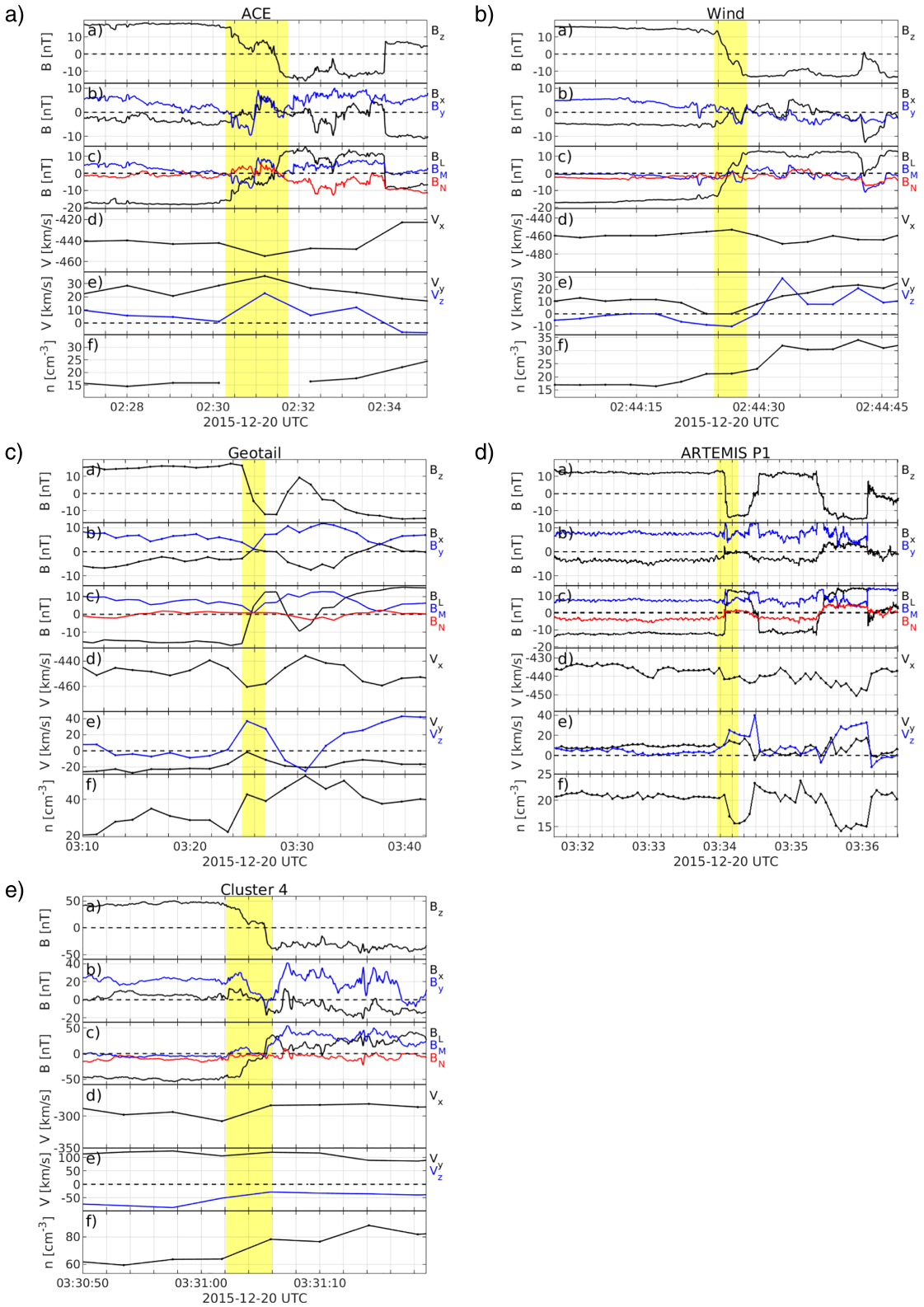

Figure 6. Observations of the DD by the ACE, Wind, Geotail, ARTEMIS P1, and Cluster 4 spacecraft. The magnetic field data are presented the GSE and the local **LMN** systems, and the velocity data in the GSE system. The approximate duration of the DD is highlighted in yellow. For the lower resolution data, the data samples are indicated with dots. Note that there is a data gap in the ACE density data at the DD.

Table 2
Time of the Observation of the DD; Spacecraft Position; Approximate Magnetic Field in GSE, Plasma Density, and Alfvén Speed Before (i) and After (f) the DD; Magnetic Field Shear Angle $\Delta\theta$; and Approximate **LMN** *Directions*

Quantity	ACE	WIND	Geotail	ARTEMIS P1	Cluster 4
UTC	02:30:54.9	02:44:26.1	03:25:40.6	03:31:04.0	03:34:04.4
R [R_E]	[240, −7.4, 25]	[195, −26, −10]	[17, 6.1, 8.4]	[−19, 53, 3.0]	[1, 13, −11]
$\mathbf{B}_i$ [nT]	[−4, 3, 17]	[−5, 3, 15]	[−3, 6, 15]	[−3, 7.5, 13]	[3, 23, 45]
$\mathbf{B}_f$ [nT]	[0, 6, −13]	[2, 0, −12]	[1, 7, −15]	[−0.3, 7.5, −14]	[−3, 27, −33]
$n_{i,f}$ [cm^{-3}]	15, 17	17, 30	30, 40	21, 16	63, 80
$V_{Ai,f}$ [km/s]	100, 76	86, 49	66, 58	74, 88	140, 110
$\Delta\theta$ [°]	140	170	130	121	110
L	[0.19, −0.038, −0.98]	[0.14 −0.23 −0.96]	[0.12, 0.06, −0.99]	[−0.06, −0.04, −1.0]	[−0.31, −0.43, −0.85]
M	[0.43, 0.90, 0.048]	[0.62, 0.78, −0.098]	[−0.33, 0.94, 0.02]	[−0.08, 1.0, −0.04]	[0.10, 0.87, −0.48]
N	[0.88, −0.43, 0.19]	[0.78, −0.58, 0.25]	[0.94, 0.32, 0.13]	[1.0, 0.07, −0.06]	[0.94, −0.24, −0.23]

of ongoing reconnection at an X-line southward of the spacecraft trajectory (Figure 3): a bifurcated current sheet showing signatures of Hall magnetic and electric fields, a normal magnetic field $B_N < 0$ indicating a magnetic connection between the two regions of the DD, field-aligned currents $J_{\|}$ similar to what is expected for Hall currents, $E_{\|}$ on the average pointing away from the X-line, and $\mathbf{E} \cdot \mathbf{J} > 0$ indicating a conversion of magnetic to kinetic energy. Moreover, the conclusion about ongoing reconnection based on the magnetic and electric fields and derived quantities (Figure 3) are strengthened by observations in subspin resolution HPCA ion energy-time spectrograms (Figure 4) where we observe indications of ions accelerated away from the X-line. The event is schematically summarized in Figure 1.

Even though MMS was unfortunately not in burst mode during our event, the survey mode electric and magnetic field data (and derived quantities) have high enough resolution for resolving the Hall fields well (Figure 3). Moreover, even though the resolution of the plasma moments is too low to be able to resolve any reconnection jets in the ion velocity data, the subspin resolution HPCA ion energy-time spectrogram data show signs of an elevated ion population consistent with ion acceleration in the ion diffusion region of reconnection (Figure 4). Hence, even though there are no high-resolution burst mode data available, we argue that the available data indicate that reconnection was likely to be ongoing southward of the MMS spacecraft.

Even though interplanetary DDs at Earth's orbit are relatively common, the probability of an Earth-orbiting spacecraft fleet crossing the thin bow shock at the same time as a DD is small. DDs typically occur once per hour at Earth's orbit (Neugebauer, 2006), the MMS orbital period is ∼1 day during the two first day-side seasons (Fuselier et al., 2016), and approximately, only half of the bow shock crossings are of a quasi-perpendicular type (for which the data are easier to interpret). Nevertheless, we have manually searched these 2-day-side seasons for similar DD events, but we have not found any. Hence, the presented event is so far the only one of its kind, and the unprecedented MMS data quality, even in survey mode without access to burst mode fields and particles data, makes it very interesting to study.

For our event, reconnection is likely to be asymmetric since the two reconnecting regions are distinctly different. The properties of asymmetric reconnection is expected to differ from the properties of the more commonly investigated case of symmetric reconnection (Eastwood et al., 2013). For example, the X-line and the stagnation point are no longer collocated for asymmetric reconnection, and the X-line is displaced away from the high mass flux side. The most commonly studied case of asymmetric reconnection is at the magnetopause (Paschmann et al., 2013). In that case, on one side (the magnetosphere), the magnetic field strength is higher and the plasma density is lower than on the other side (the magnetosheath). In the bow shock example presented in this article, on the other hand, both the magnetic field and the plasma density are high on one side (the magnetosheath) and low on the other side (the solar wind). At the solar wind side, the plasma flow is even supersonic.

Indeed, our event shows deviations from the typical behavior of symmetric reconnection. For example, the bifurcated current sheet is asymmetric and the part facing the magnetosheath is steeper as compared to the one facing the undisturbed solar wind. Moreover, the region closest to a magnetic null is displaced away from

the solar wind side, and observations of the out-of-plane electric field E_M indicate that the the reconnection inflow is mainly from the solar wind side. Asymmetric reconnection at the magnetopause has been studied before with numerical simulations, and observed data have been compared with simulation results (see for example Eastwood et al., 2013, and references therein). However, for asymmetric reconnection of the bow shock case, there are presently no available numerical simulations to compare with.

Reconnection has previously been observed in current sheets upstream the bow shock (e.g., Gosling, 2012) as well as in the turbulent downstream magnetosheath (e.g., Eriksson et al., 2018; Maynard et al., 2007; Phan et al., 2007, 2018; Retinò et al., 2007; Vörös et al., 2017; Wilder et al., 2017, 2018). Moreover, reconnection has also been observed in the turbulent plasma in the transition region of quasi-parallel bow shocks, just behind the ramp before the plasma is fully decelerated to the downstream flow (Gingell et al., 2019; Wang et al., 2018). In the cases discussed by Wang et al. (2018) and Gingell et al. (2019), reconnection is suggested to arise spontaneously in nonstationary and turbulent shock structures. On the other hand, the event presented in this article is suggested to be caused by an external driver in the form of a compression of a DD in the region just behind the ramp. To our knowledge, this is the first observation of externally driven reconnection near the bow shock ramp and it offers favorable conditions for investigating specifically asymmetric reconnection in other plasma regimes than previously investigated, for example, at the magnetopause.

The observed event raises the question if reconnection can be triggered as an interplanetary DD is compressed by the bow shock. Did reconnection only occur temporarily at the observed DD as it crossed the bow shock, or did reconnection already occur at the DD in the pristine solar wind and continued as it crossed the shock? The DD is observed by four missions upstream the bow shock, ACE, WIND, Geotail, and ARTEMIS, and by Cluster in the downstream magnetosheath (Figures 5 and 6). The DD can easily be discerned from the magnetic field data of the five spacecraft, and at least for ACE and Cluster the current sheet is bifurcated (for Geotail, however, the resolution of the magnetic field data is too low to be ably to conclude if the current sheet is bifurcated). Reconnection in the solar wind should be recognized as approximately Alfvénic accelerated plasma jets embedded in a bifurcated current sheet (see Gosling, 2012, and references therein). The approximate Alfvén speed at the five spacecraft is listed in Table 2. None of the spacecraft in Figure 6 show any indications of Alfvénic accelerated jets, although it should be noted that the resolution of the plasma moment data is low. However, at least for ACE, WIND, and ARTEMIS, the velocity moment has samples inside the DD, but still we see no indications of an increased speed of the order of the Alfvén speed. We therefore suggest that reconnection did not occur in the pristine solar wind or in the magnetosheath, but it was temporarily triggered as the DD crossed and was compressed by the bow shock.

Acknowledgments
M. H. and A. D. S. were supported by the Swedish National Space Agency (SNSA), H. G. by the Belgian Science Policy Office through the Solar Terrestrial Centre of Excellence and the PRODEX/Cluster contract 13127/98/NL/VJ(IC)-PEA90316, and O. G. by the Kempe foundations. We thank the MMS Science Data Center and all the MMS teams, especially the magnetic field and the ion teams, in producing high-quality data. We also acknowledge NASA's National Space Science Data Center and Space Physics Data Facility. All data are available trough https://lasp.colorado.edu/mms/sdc/public/, https://cdaweb.gsfc.nasa.gov, and https://www.cosmos.esa.int/web/csa.

References

Angelopoulos, V. (2008). The THEMIS Mission. *Space Science Reviews*, *141*, 5–34. https://doi.org/10.1007/s11214-008-9336-1

Angelopoulos, V., McFadden, J. P., Larson, D., Carlson, C. W., Mende, S. B., Frey, H., et al. (2008). Tail reconnection triggering substorm onset. *Science*, *321*, 931. https://doi.org/10.1126/science.1160495

Auster, H. U., Glassmeier, K. H., Magnes, W., Aydogar, O., Baumjohann, W., Constantinescu, D., et al. (2008). The THEMIS fluxgate magnetometer. *Space Science Reviews*, *141*, 235–264. https://doi.org/10.1007/s11214-008-9365-9

Bagdonat, T., & Motschmann, U. (2002). From a weak to a strong comet—3D global hybrid simulation studies. *Earth Moon Plan*, *90*, 305–321. https://doi.org/10.1023/A:1021578232282

Bale, S. D., Balikhin, M. A., Horbury, T. S., Krasnoselskikh, V. V., Kucharek, H., Möbius, E., et al. (2005). Quasi-perpendicular shock structure and processes. *Space Science Reviews*, *118*, 161–203. https://doi.org/10.1007/s11214-005-3827-0

Balogh, A., Carr, C. M., Acuña, M. H., Dunlop, M. W., Beek, T. J., Brown, P., et al. (2001). The cluster magnetic field investigation: Overview of in-flight performance and initial results. *Annales Geophysicae*, *19*, 1207–1217. https://doi.org/10.5194/angeo-19-1207-2001

Bessho, N., Chen, L., Wang, S., Hesse, M., & Wilson, L. (2019). Magnetic reconnection in a quasi-parallel shock: Two-dimensional local particle-in-cell simulation. *Geophysical Research Letters*, *46*, 9352–9361. https://doi.org/10.1029/2019GL083397

Bohdan, A., Niemiec, J., Kobzar, O., & Pohl, M. (2017). Electron pre-acceleration at nonrelativistic high-mach-number perpendicular shocks. *The Astrophysical Journal*, *847*(1), 71. https://doi.org/10.3847/1538-4357/aa872a

Burch, J. L., Moore, T. E., Torbert, R. B., & Giles, B. L. (2015). Magnetospheric multiscale overview and science objectives. *Space Science Reviews*, *199*, 5–21. https://doi.org/10.1007/s11214-015-0164-9

Burch, J. L., & Phan, T. D. (2016). Magnetic reconnection at the dayside magnetopause: Advances with MMS. *Geophysical Research Letters*, *43*, 8327–8338. https://doi.org/10.1002/2016GL069787

Drake, J. F., Swisdak, M., Phan, T. D., Cassak, P. A., Shay, M. A., Lepri, S. T., et al. (2009). Ion heating resulting from pickup in magnetic reconnection exhausts. *Journal of Geophysical Research*, *114*, A05111. https://doi.org/10.1029/2008JA013701

Dungey, J. W. (1961). Interplanetary magnetic field and the auroral zones. *Physical Review Letters*, *6*, 47–48. https://doi.org/10.1103/PhysRevLett.6.47

Dunlop, M. W., Balogh, A., Glassmeier, K.-H., & Robert, P. (2002). Four-point cluster application of magnetic field analysis tools: The Curlometer. *Journal of Geophysical Research*, *107*(A11), 1384. https://doi.org/10.1029/2001JA005088

Eastwood, J. P., Bale, S. D., Mozer, F. S., & Hull, A. J. (2007). Contributions to the cross shock electric field at a quasiperpendicular collisionless shock. *Geophysical Research Letters*, L17104. https://doi.org/10.1029/2007GL030610

Eastwood, J. P., Mistry, R., Phan, T. D., Schwartz, S. J., Ergun, R. E., Drake, J. F., et al. (2018). Geophysical research letters, *45*, 4569–4577. https://doi.org/10.1029/2018GL077670

Eastwood, J. P., Phan, T. D., Øieroset, M., Shay, M. A., Malakit, K., Swisdak, M., et al. (2013). Influence of asymmetries and guide fields on the magnetic reconnection diffusion region in collisionless space plasmas. *Plasma Physics and Controlled Fusion*, *55*(12), 124001. https://doi.org/10.1088/0741-3335/55/12/124001

Ergun, R. E., Tucker, S., Westfall, J., Goodrich, K. A., Malaspina, D. M., Summers, D., et al. (2016). The axial double probe and fields signal processing for the MMS mission. *Space Science Reviews*, *199*, 167–188. https://doi.org/167--18810.1007/s11214-014-0115-x

Eriksson, E., Vaivads, A., Graham, D. B., Divin, A., Khotyaintsev, Y. V., Yordanova, E., et al. (2018). Electron energization at a reconnecting magnetosheath current sheet. *Geophysical Research Letters*, *45*, 8081–8090. https://doi.org/10.1029/2018GL078660

Escoubet, C. P., Fehringer, M., & Goldstein, M. (2001). Introduction: The cluster mission. *Annales Geophysicae*, *19*, 1197–1200. https://doi.org/10.5194/angeo-19-1197-2001

Farris, M. H., & Russell, C. T. (1994). Determining the standoff distance of the bow shock: Mach number dependence and use of models. *Journal of Geophysical Research*, *99*, 17,681–17,689. https://doi.org/10.1029/94JA01020

Frank, L. A., Ackerson, K. L., Paterson, W. R., Lee, J. A., English, M. R., & Pickett, G. L. (1994). The comprehensive plasma instrumentation (CPI) for the GEOTAIL spacecraft. *Journal of Geomagnetism Geoelectricity*, *46*, 23–37. https://doi.org/10.5636/jgg.46.23

Fuselier, S. A., Lewis, W. S., Schiff, C., Ergun, R., Burch, J. L., Petrinec, S. M., & Trattner, K. J. (2016). Magnetospheric multiscale science mission profile and operations. *Space Science Reviews*, *199*, 77–103. https://doi.org/10.1007/s11214-014-0087-x

Gingell, I., Schwartz, S. J., Burgess, D., Johlander, A., Russell, C. T., Burch, J. L., et al. (2017). MMS observations and hybrid simulations of surface ripples at a marginally quasi-parallel shock. *Journal of Geophysical Research: Space Physics*, *122*, 11,003–11,017. https://doi.org/10.1002/2017JA024538

Gingell, I., Schwartz, S. J., Eastwood, J. P., Burch, J. L., Ergun, R. E., Fuselier, S., et al. (2019). Observations of magnetic reconnection in the transition region of quasi-parallel shocks. *Geophysical Research Letters*, *46*, 1177–1184. https://doi.org/10.1029/2018GL081804

Gosling, J. T. (2012). Magnetic reconnection in the solar wind. *Space Science Reviews*, *172*, 187–200. https://doi.org/10.1007/s11214-011-9747-2

Johlander, A., Schwartz, S. J., Vaivads, A., Khotyaintsev, Y. V., Gingell, I., Peng, I. B., et al. (2016). Rippled quasiperpendicular shock observed by the Magnetospheric Multiscale spacecraft. *Physical Review Letters*, *117*(16), 165101. https://doi.org/10.1103/PhysRevLett.117.165101

Kokubun, S., Yamamoto, T., Acuña, M. H., Hayashi, K., Shiokawa, K., & Kawano, H. (1994). The GEOTAIL magnetic field experiment. *Journal of Geomagnetism Geoelectricity*, *46*, 7–21. https://doi.org/10.5636/jgg.46.7

Lepping, R. P., Acũna, M. H., Burlaga, L. F., Farrell, W. M., Slavin, J. A., Schatten, K. H., et al. (1995). The wind magnetic field investigation. *Space Science Reviews*, *71*, 207–229. https://doi.org/10.1007/BF00751330

Lin, Y. (1997). Generation of anomalous flows near the bow shock by its interaction with interplanetary discontinuities. *Journal of Geophysical Research*, *102*, 24,265–24,282. https://doi.org/10.1029/97JA01989

Lin, R. P., Anderson, K. A., Ashford, S., Carlson, C., Curtis, D., Ergun, R., et al. (1995). A three-dimensional plasma and energetic particle investigation for the wind spacecraft. *Space Science Reviews*, *71*, 125–153. https://doi.org/10.1007/BF00751328

Lindkvist, J., Hamrin, M., Gunell, H., Nilsson, H., Simon Wedlun, C., Kallio, E., et al. (2018). Energy conversion in cometary atmospheres—Hybrid modeling of 67P/Churyumov-Gerasimenko. *Astronomy & Astrophysics*, *616* A81. https://doi.org/10.1051/0004-6361/201732353

Lindqvist, P.-A., Olsson, G., Torbert, R. B., King, B., Granoff, M., Rau, D., et al. (2016). The spin-plane double probe electric field instrument for MMS. *Space Science Reviews*, *199*, 137–165. https://doi.org/10.1007/s11214-014-0116-9

Matsumoto, Y., Amano, T., Kato, T. N., & Hoshino, M. (2015). Stochastic electron acceleration during spontaneous turbulent reconnection in a strong shock wave. *Science*, *347*(6225), 974–978. https://doi.org/10.1126/science.1260168

Maynard, N. C., Burke, W. J., Ober, D. M., Farrugia, C. J., Kucharek, H., Lester, M., et al. (2007). Interaction of the bow shock with a tangential discontinuity and solar wind density decrease: Observations of predicted fast mode waves and magnetosheath merging. *Journal of Geophysical Research*, *112*, A12219. https://doi.org/10.1029/2007JA012293

Maynard, N. C., Sonnerup, B. U. Ö, Siscoe, G. L., Weimer, D. R., Siebert, K. D., Erickson, G. M., et al. (2002). Predictions of magnetosheath merging between IMF field lines of opposite polarity. *Journal of Geophysical Research*, *107*(A12), 1456. https://doi.org/10.1029/2002JA009289

McComas, D. J., Bame, S. J., Barker, P., Feldman, W. C., Phillips, J. L., Riley, P., & Griffee, J. W. (1998). Solar wind electron proton alpha monitor (SWEPAM) for the advanced composition explorer. *Space Science Reviews*, *86*, 563–612. https://doi.org/10.1023/A:1005040232597

McFadden, J. P., Carlson, C. W., Larson, D., Bonnell, J., Mozer, F., Angelopoulos, V., et al. (2008). THEMIS ESA first science results and performance issues. *Space Science Reviews*, *141*, 477–508. https://doi.org/10.1007/s11214-008-9433-1

Mistry, R., Eastwood, J. P., Haggerty, C. C., Shay, M. A., Phan, T. D., Hietala, H., & Cassak, P. A. (2016). Observations of hall reconnection physics far downstream of the X line. *Physical Review Letters*, *117*(18), 185102. https://doi.org/10.1103/PhysRevLett.117.185102

Neugebauer, M. (2006). Comment on the abundances of rotational and tangential discontinuities in the solar wind. *Journal of Geophysical Research*, *111*, A04103. https://doi.org/10.1029/2005JA011497

Paschmann, G., Haerendel, G., Sckopke, N., Möbius, E., Lühr, H., & Carlson, C. W. (1988). Three-dimensional plasma structures with anomalous flow directions near the Earth's bow shock. *Journal of Geophysical Research*, *93*, 11,279–11,294. https://doi.org/10.1029/JA093iA10p11279

Paschmann, G., Øieroset, M., & Phan, T. (2013). In-situ observations of reconnection in space. *Space Science Reviews*, *178*, 385–417. https://doi.org/10.1007/s11214-012-9957-2

Paschmann, G., & Schwartz, S. J. (2000). ISSI Book on analysis methods for multi-spacecraft data. In R. A. Harris (Ed.), *Cluster-II Workshop Multiscale / Multipoint Plasma Measurements* (Vol. 449, pp. 99). London, UK: ESA Special Publication.

Phan, T. D., Eastwood, J. P., Shay, M. A., Drake, J. F., Sonnerup, B. U. Ö., Fujimoto, M., et al. (2018). Electron magnetic reconnection without ion coupling in Earth's turbulent magnetosheath. *Nature*, *557*, 202–206. https://doi.org/10.1038/s41586-018-0091-5

Phan, T. D., Love, T. E., Gosling, J. T., Paschmann, G., Eastwood, J. P., Oieroset, M., et al. (2011). Triggering of magnetic reconnection in a magnetosheath current sheet due to compression against the magnetopause. *Geophysical Research Letters*, *38*, L17101. https://doi.org/10.1029/2011GL048586

Phan, T. D., Paschmann, G., Twitty, C., Mozer, F. S., Gosling, J. T., Eastwood, J. P., et al. (2007). Evidence for magnetic reconnection initiated in the magnetosheath. *Geophysical Research Letters*, *34*, L14104. https://doi.org/10.1029/2007GL030343

Pollock, C., Moore, T., Jacques, A., Burch, J., Gliese, U., Saito, Y., et al. (2016). Fast plasma investigation for magnetospheric multiscale. *Space Science Reviews*, *199*, 1–76. https://doi.org/10.1007/s11214-016-0245-4

Priest, E. R., & Forbes, T. G. (2002). The magnetic nature of solar flares. *The Astronomy and Astrophysics Review*, *10*, 313–377. https://doi.org/10.1007/s001590100013

Pritchett, P. L. (2008). Collisionless magnetic reconnection in an asymmetric current sheet. *Journal of Geophysical Research*, *113*, A06210. https://doi.org/10.1029/2007JA012930

Pritchett, P. L., & Mozer, F. S. (2009). Asymmetric magnetic reconnection in the presence of a guide field. *Journal of Geophysical Research*, *114*, A11210. https://doi.org/10.1029/2009JA014343

Rème, H., Aoustin, C., Bosqued, J. M., Dandouras, I., Lavraud, B., Sauvaud, J. A., et al. (2001). First multispacecraft ion measurements in and near the Earth's magnetosphere with the identical Cluster ion spectrometry (CIS) experiment. *Annales Geophysicae*, *19*, 1303–1354. https://doi.org/10.5194/angeo-19-1303-2001

Retinò, A., Sundkvist, D., Vaivads, A., Mozer, F., André, M., & Owen, C. J. (2007). In situ evidence of magnetic reconnection in turbulent plasma. *Nature*, *3*, 236–238. https://doi.org/10.1038/nphys574

Russell, C. T., Anderson, B. J., Baumjohann, W., Bromund, K. R., Dearborn, D., Fischer, D., et al. (2014). The magnetospheric multiscale magnetometers. *Space Science Reviews*. https://doi.org/10.1007/s11214-014-0057-3

Saxena, R., Bale, S. D., & Horbury, T. S. (2005). Wavelength and decay length of density overshoot structure in supercritical, collisionless bow shocks. *Physics of Plasmas*, *12*(5), 052,904–052,904. https://doi.org/10.1063/1.1900093

Schwartz, S. J. (1998). Shock and discontinuity normals, mach numbers, and related parameters. *ISSI Scientific Reports Series*, *1*, 249–270.

Schwartz, S. J., Paschmann, G., Sckopke, N., Bauer, T. M., Dunlop, M., Fazakerley, A. N., & Thomsen, M. F. (2000). Conditions for the formation of hot flow anomalies at Earth's bow shock. *J. Geophys. Res.*, *105*, 12,639–12,650. https://doi.org/10.1029/1999JA000320

Shue, J.-H., Chao, J. K., Fu, H. C., Russell, C. T., Song, P., Khurana, K. K., & Singer, H. J. (1997). A new functional form to study the solar wind control of the magnetopause size and shape. *Journal of Geophysical Research*, *102*, 9497–9512. https://doi.org/10.1029/97JA00196

Smith, C. W., L'Heureux, J., Ness, N. F., Acuña, M. H., Burlaga, L. F., & Scheifele, J. (1998). The ACE Magnetic Fields Experiment. *Space Science Reviews*, *86*, 613–632. https://doi.org/10.1023/A:1005092216668

Thomsen, M. F., Gosling, J. T., Fuselier, S. A., Bame, S. J., & Russell, C. T. (1986). Hot, diamagnetic cavities upstream from the Earth's bow shock. *Journal of Geophysical Research*, *91*(A3), 2961–2974. https://doi.org/10.1029/JA091iA03p02961

Torbert, R. B., Russell, C. T., Magnes, W., Ergun, R. E., Lindqvist, P.-A., LeContel, O., et al. (2014). The FIELDS instrument suite on MMS: Scientific objectives, measurements, and data products. *Space Science Reviews*, *199*, 105–135. https://doi.org/10.1007/s11214-014-0109-8

Vernisse, Y., Riousset, J. A., Motschmann, U., & Glassmeier, K.-H. (2018). Simulations of stellar winds and planetary bodies: Magnetized obstacles in a super-Alfvénic flow with southward IMF. *Planetary and Space Science*, *152*, 18–30. https://doi.org/10.1016/j.pss.2018.01.010

Vörös, Z., Yordanova, E., Varsani, A., Genestreti, K. J., Khotyaintsev, Y. V., Li, W., et al. (2017). MMS observation of magnetic reconnection in the turbulent magnetosheath. *Journal of Geophysical Research: Space Physics*, *122*, 11,442–11,467. https://doi.org/10.1002/2017JA024535

Wang, S., Chen, L.-J., Bessho, N., Hesse, M., Wilson III, L. B., Giles, B., et al. (2018). Observational evidence of magnetic reconnection in the terrestrial bow shock transition region. *Geophysical Research Letters*, *46*, 562–570. https://doi.org/10.1029/2018GL080944

Wang, L., Hakim, A. H., Bhattacharjee, A., & Germaschewski, K. (2015). Comparison of multi-fluid moment models with particle-in-cell simulations of collisionless magnetic reconnection. *Phys. Plasmas*, *22*(1), 012108. https://doi.org/10.1063/1.4906063

Wilder, F. D., Ergun, R. E., Burch, J. L., Ahmadi, N., Eriksson, S., Phan, T. D., et al. (2018). The role of the parallel electric field in electron-scale dissipation at reconnecting currents in the magnetosheath. *Journal of Geophysical Research: Space Physics*, *123*, 6533–6547. https://doi.org/10.1029/2018JA025529

Wilder, F. D., Ergun, R. E., Eriksson, S., Phan, T. D., Burch, J. L., Ahmadi, N., et al. (2017). Multipoint measurements of the electron jet of symmetric magnetic reconnection with a moderate guide field. *Physical Review Letters*, *118*(26), 265101. https://doi.org/10.1103/PhysRevLett.118.265101

Yamada, M., Yoo, J., Jara-Almonte, J., Ji, H., Kulsrud, R. M., & Myers, C. E. (2014). Conversion of magnetic energy in the magnetic reconnection layer of a laboratory plasma. *Nature*, *5*, 4774. https://doi.org/10.1038/ncomms5774

Young, D. T., Burch, J. L., Gomez, R. G., De Los Santos, A., Miller, G. P., Wilson, P., et al. (2016). Hot plasma composition analyzer for the magnetospheric multiscale mission. *Space Science Reviews*, *199*, 407–470. https://doi.org/10.1007/s11214-014-0119-6

Zhao, L. L., Zhang, H., & Zong, Q.-G. (2017). A statistical study on hot flow anomaly current sheets. *Journal of Geophysical Research: Space Physics*, *122*, 235–248. https://doi.org/10.1002/2016JA023319